



Correlation Between Constituent Phase and Weld Metal Properties in Ni-Reduced Duplex Stainless Steel

Youngchai Lee¹ · Jae Hee Lee¹ · Joonoh Moon² · Tae-Ho Lee² · Changhee Lee¹

Received: 30 March 2021 / Accepted: 9 July 2021 / Published online: 15 December 2021
© The Korean Institute of Metals and Materials 2021

Abstract

The intrinsic properties of austenite and ferrite on the mechanical properties and corrosion resistance of the duplex stainless steel weld metals was studied by substituting Ni with Mn, N, and Mn+N. The properties of the weldments fabricated through gas tungsten arc welding (GTAW) were evaluated using tensile test, Vickers hardness, and potentiodynamic polarization tests. The mechanical properties and corrosion resistance of the constituent phases were measured using nanoindentation and electron probe microanalysis, respectively. The austenite and ferrite phase fractions of the weld metal were maintained at approximately 50:50, and no harmful phases degraded the properties. Excessive Mn decreased the corrosion resistance; a large difference in corrosion resistance between austenite and ferrite also decreased the overall corrosion resistance. In the filler metal in which Ni was replaced with only Mn or N, the austenite became harder than ferrite, as a result cracks initiated inside the austenite. The tensile test showed that austenite, which became a relatively hard phase compared to ferrite according to the chemical composition, increased the yield strength and decreased the elongation of the weld metal.

Keywords Duplex stainless steel · Weld metal · Nanoindentation · Mechanical property · Corrosion resistance

1 Introduction

Duplex stainless steel (DSS) have been used in various fields such as chemical, petrochemical, and offshore plants owing to its excellent mechanical properties and corrosion resistance [1–5]. This excellent characteristic of DSS comes from the complex microstructure consisting of austenite with good ductility and general corrosion resistance and ferrite with high strength at fraction of approximately 50:50 [6–10]. The best properties of DSS are obtained when the fraction of austenite and ferrite is about 50:50, so it is important to carefully control the heat treatment temperature and time to maintain the fraction of austenite and ferrite, while suppressing secondary phases such as sigma (σ) or chi (χ) and precipitates such as chromium carbide and nitride which degrade mechanical properties and corrosion resistance.

In general, for obtaining proper phase fraction and controlling the deleterious phases in DSS, 5–20 kJ/cm heat input is recommended [11, 12]. The low heat input causes a fast cooling rate, increases the ferrite content of the weldment, and may precipitate chromium carbide and nitride. On the contrary, the high heat input result in a slow cooling rate, and brittle secondary phases may be precipitated due to prolonged exposure to 600–1000 °C. [13–16].

To solve this problem, a filler wire with Ni content 2%–4% higher than that of the base metal has generally been used [3, 17, 18]. Ni addition maintains the austenite fraction of the DSS weld but increases the production cost due to the high price of Ni and price instability. Therefore, many researches have been conducted to replace the Ni in DSS. In these studies, it is reported that Mn and N are the most preferred elements to replace Ni [19–21]. Mn and N are known to be strong austenite stabilizers and have the advantage of being relatively more cost-effective than Ni. However, Mn and N have some disadvantage depending on the chemical composition of steel. Mn is generally known as an alloying element that degrades corrosion resistance [22], and deteriorates weldability in high-manganese steels [23]. When N is precipitated as chromium nitride, Cr depleted zone is formed around the nitride, reducing corrosion resistance

✉ Changhee Lee
chlee@hanyang.ac.kr

¹ Division of Materials Science and Engineering, Hanyang University, Seoul 04763, Republic of Korea

² Ferrous Alloy Department, Korea Institute of Materials Science, Changwon 51508, Republic of Korea

[24]. Therefore, it is important to control the alloy composition when trying to replace Ni with Mn and N.

Many studies have been conducted to determine the effects of Mn and N in DSS. However, since Mn and N were added while maintaining the Ni content, the phase fractions of the weld changed. As a result, most studies explain changes in properties in terms of the phase fraction [25–29]. As mentioned above, DSS is known to exhibit the best properties when the fraction of austenite and ferrite is maintained at approximately 50:50; therefore, the effect of replacing Ni with Mn and N while maintaining the phase fraction must be studied.

In this study, the mechanical properties and corrosion resistance of the weld metal according to the intrinsic properties of austenite and ferrite while maintaining the phase fraction were investigated. Based on ER2209 (Fe–22Cr–9Ni–3Mo–1.5Mn–0.15N), a filler metal used in standard grade DSS, five filler metals were designed in which Ni was replaced with Mn, N, and Mn + N. Tensile and Vickers hardness tests were performed to measure the mechanical properties of the weld metal, and the corrosion resistance was measured using the potentiodynamic polarization test. In addition, the mechanical properties of constituent phases were measured through nanoindentation tests, and the corrosion resistance was inferred from the pitting resistance equivalent number (PREN, $\text{Cr} + 3.3\text{Mo} + 16\text{N} - \text{Mn}$) [30] values of each phase. From results, the correlation between constituent phases and weld metal properties were investigated, and the possibility of replacing Ni with Mn and N was suggested.

2 Experimental Methods

Table 1 indicates the chemical compositions of the alloys used in this investigation. Based on the commercial duplex stainless steel filler metal, ER2209 (Fe–22Cr–9Ni–3Mo–1.5Mn–0.15 N, wt%), five alloys were designed in which Ni was replaced with Mn, N, and Mn + N. The contents of Ni, Mn, and N were adjusted to have austenite stability similar to that of ER2209 based on the Ni equivalent ($\text{Ni}_{\text{eq}}, \text{Ni} + 30\text{C} + 30\text{N} + 0.5\text{Mn}$ in the Delong

diagram) [31]. In addition, based on the calculation results using Thermo-Calc (TCFE2) simulation software, the alloy compositions were designed to have a phase fraction similar to that of ER2209 (Fig. 1).

Each designed alloy was manufactured as a cast ingot with a total weight of 1700 g using a vacuum induction furnace at 100% Ar and a pressure of 1 bar. Cast materials (Fe, Cr, Ni, Mo, and Mn) were prepared with high purity above 99.7%, and 60Cr–32.5Fe–7.5 N (in wt%) powder was used to control the nitrogen content. The chemical composition of the ingot was measured using optical emission spectroscopy (QSN 750-II) and an N/O analyzer (LECO, TC-436). The fabricated alloys were machined to a thickness of 6 mm, and bead-on-plate gas tungsten arc welding (GTAW) was performed on the processed plate to simulate the weld metals. The welding conditions were set so as not to exceed the heat input range generally used for duplex stainless steel, and the detailed parameters are as follows; voltage: 17 V, current: 180 A, travel speed: 18 cm/min, shielding gas (Ar) flow: 15 L/min, working distance: 2 mm and heat input: 10 kJ/cm.

Figure 2 shows a schematic of the tensile test specimen. To exclude the influence of the base metal and heat-affected zone (HAZ) on the tensile test results, the tensile specimen was fabricated so that the gauge length part became an all-weld metal, as shown in Fig. 2. Tensile tests were

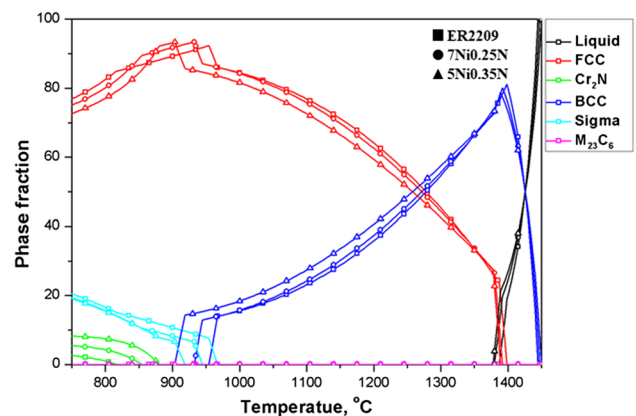


Fig. 1 Equilibrium phase fractions of ER2209, 7Ni0.25N, 5Ni0.35N calculated using Thermo-Calc. software

Table 1 Chemical compositions of the duplex stainless steel filler metal

Materials	Composition (wt%)						
	Fe	C	Cr	Mo	Ni	Mn	N
ER2209	Bal.	0.002	22.2	2.87	9.2	1.39	0.15
7Ni8.5Mn	Bal.	0.002	21.94	2.99	7.4	8.38	0.15
7Ni0.25N	Bal.	0.002	22.35	2.88	7.07	1.4	0.25
5Ni0.35N	Bal.	0.002	21.9	2.89	4.9	1.34	0.35
5Ni6.5Mn0.25N	Bal.	0.002	22.14	2.78	5.03	6.48	0.25
3Ni6.5Mn0.35N	Bal.	0.002	21.96	2.97	3.13	6.26	0.35

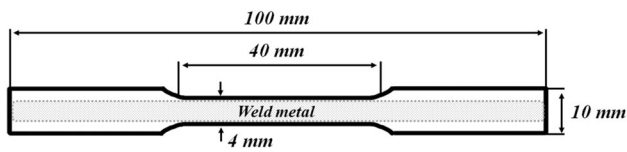


Fig. 2 Schematic image and dimension of the tensile test specimen

conducted at room temperature using a universal testing machine (ZWICK Z100-ZWICK). The test was performed under the conditions of 10^{-3} per second strain rate. After the tensile tests were completed, the cross section of the tested specimens was observed via a scanning electron microscope (SEM) to analyze the crack formation. To observe the crack initiation site, the microstructure was observed right next to the fracture. The hardness of the weld metals was measured using a Vickers hardness machine (HMV-2, Shimadzu) with a 1.96 N load and 5 s dwelling time. The microhardness values were measured 20 times for each specimen, and the average value was used. Moreover, nanoindentation tests were performed using a three-sided pyramidal Berkovich indenter to measure the austenite and ferrite hardness. The applied load and strain rate were 10 mN and 0.05/s, respectively, and the holding time, which indicates the duration time at peak load, was 1 s. After indentation at 30 μm intervals between points, only data on indentations imprinted on austenite or ferrite were used.

To estimate the corrosion resistance properties, a potentiodynamic polarization test was conducted at 25 $^{\circ}\text{C}$ using a potentiostat instrument (EG&G model 273A). All other surfaces except the weld metals were covered with masking tape to prevent contact with the test solution. 1 M NaCl + 0.5 M

HCl solution was used as the test solution, and Ag/AgCl and platinum rod were used as the reference electrode and the counter electrode, respectively.

The alloys were mechanically polished using SiC paper up to 2000 grit and micropolished using a 1 μm diamond suspension. Thereafter, the microstructure was revealed by electrochemical etching in a 60% HNO_3 + 40% H_2O solution, and microstructural observations were performed using a field emission scanning electron microscope (FE-SEM, Carl Zeiss, SIGMA) working at 20 kV. The phase fraction was measured using an image analyzer software, and the presence or absence of precipitates and secondary phases such as sigma phase was confirmed using X-ray diffraction (XRD, SmartLab, Rigaku, Japan). XRD was carried out for as-welded specimens with angle 20° to 80° under 45 kV and 200 mA conditions and $\text{Cu K}\alpha$ radiation. The chemical compositions of the austenite and ferrite were measured using electron probe micro-analysis (EPMA, JXA-8530F, JEOL).

3 Results and Discussion

3.1 Microstructural Characteristics

Figure 3 shows the microstructures of the weld metal of the commercial filler metal ER2209 and the developed filler metal in which Ni was replaced with Mn and N. In all filler metals, grain boundary austenite (GBA), Widmanstätten austenite (WA), and intragranular austenite (IGA) were observed in the ferrite matrix, which are typically found in duplex stainless steel welds. As shown in Fig. 3, there were no precipitates such as Cr_2N or secondary phases such as

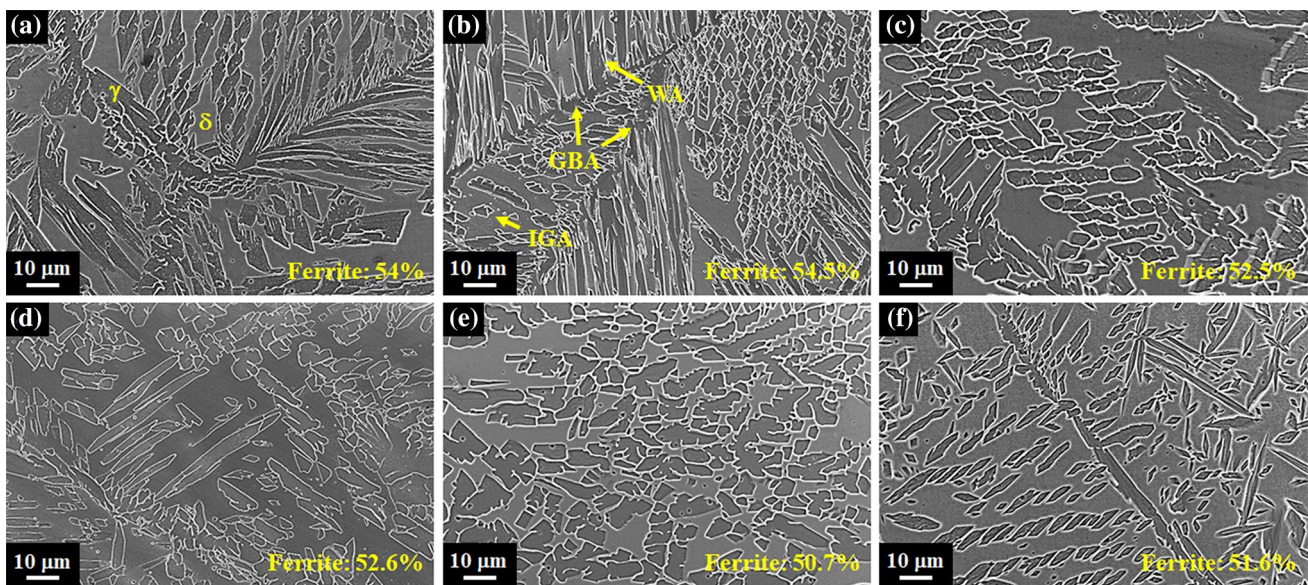


Fig. 3 Microstructure of as welded filler metal **a** ER2209, **b** 7Ni8.5Mn, **c** 7Ni0.25N, **d** 5Ni0.35N, **e** 5Ni6.5Mn0.25N and **f** 3Ni6.5Mn0.35N

sigma and chi, which are known to degrade the mechanical properties and corrosion resistance of duplex stainless steel. Using an image analyzer, the ferrite content in the weld metals was measured to be 50.7%–54.5%, and because the austenite and ferrite ratio was approximately 50:50, the difference in properties due to the phase fraction would not be significant. Figure 4 shows the results of the X-ray diffraction (XRD) analysis of the weld metals. As shown in the SEM observations, there were no phases other than austenite and ferrite. Because the cooling rate was neither too fast nor too slow because of the appropriate heat input according to the welding conditions, the ratio of austenite and ferrite could be maintained at approximately 50:50 while controlling the precipitation of harmful phases. In other words, the difference in properties is determined only by the intrinsic properties of constituent phases because there was no phase

fraction change and harmful phases, which were generally known to cause deterioration of mechanical properties and corrosion resistance of DSS. Table 2 shows the chemical compositions of each austenite and ferrite, measured using EPMA. Overall, the ferrite stabilizer Cr was rich in ferrite and austenite stabilizer Ni and Mn were rich in austenite, but the content difference between austenite and ferrite was not large. This is because the cooling rate after welding is not fast enough to break the austenite/ferrite phase fraction, but fast enough to prevent redistribution of substitutional alloying elements with slow diffusion rate, such as Cr, Ni and Mn. In a similar vein, even though Mo is a ferrite stabilizer, its diffusion rate is so slow that almost the same content was distributed in austenite and ferrite. On the other hand, in the case of N, which is considered as an austenite stabilizer with a fast diffusion rate, it was hardly found in ferrite but was rich in austenite. In addition, because N is not soluble in ferrite at room temperature, most of the N was distributed in austenite, so it contained twice the total N content.

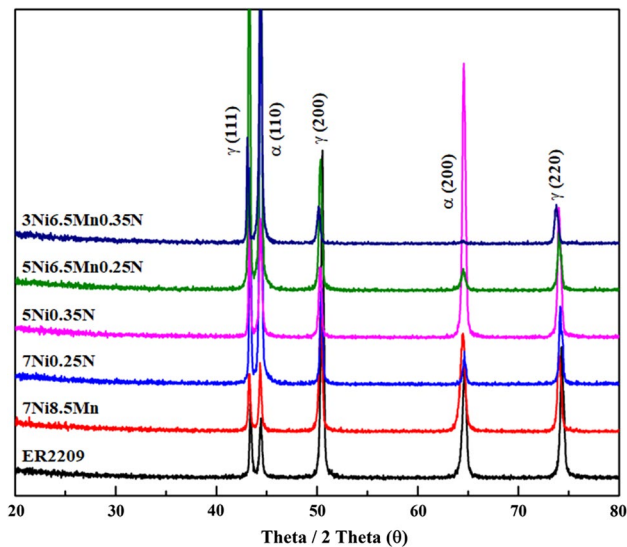


Fig. 4 X-ray diffraction spectra of the as-welded filler metal sample

3.2 Corrosion and Mechanical Properties

Figure 5 and Table 3 show the potentiodynamic polarization test curves and results of corrosion properties; experiments were performed in a 1 M NaCl + 0.5 M HCl solution. In all filler metals, the passive region where the current did not increase explosively was similar to about 0.1–1.15 V, indicating that the tendency to form a passive film was similar. The values of I_{pass} , which is considered to have better corrosion resistance as the value is lower, were observed from 5.05×10^{-6} to 1.94×10^{-5} A/cm². ER2209, a commercial filler metal, had the lowest I_{pass} and among the developed filler metals, 5Ni6.5Mn0.25N had the lowest I_{pass} and 7Ni8.5Mn had the highest value. It was reasonable that 7Ni8.5Mn, which contained the most Mn that reduces PREN, had the highest I_{pass} . However, among the

Table 2 Chemical compositions of the ferrite (δ) and austenite (γ) of DSS filler metal which measured using an EPMA

Materials	Phase	Composition (wt%)					
		Fe	Cr	Mo	Ni	Mn	N
ER2209	δ	65.29	23.10	2.95	8.74	1.53	0.01
	γ	64.87	22.81	2.92	9.08	1.56	0.27
7Ni8.5Mn	δ	60.69	22.94	2.93	6.91	8.03	0.02
	γ	60.43	22.48	2.73	7.34	8.30	0.35
7Ni0.25N	δ	67.29	23.33	2.97	6.78	1.76	0.02
	γ	66.74	23.15	2.85	6.90	1.76	0.49
5Ni0.35N	δ	69.34	23.16	2.93	4.89	1.47	0.02
	γ	69.32	22.95	2.88	5.08	1.52	0.65
5Ni6.5Mn0.25N	δ	65.19	22.68	3.04	4.89	6.04	0.05
	γ	65.10	22.51	2.80	5.04	6.10	0.50
3Ni6.5Mn0.35N	δ	65.24	24.33	2.92	2.98	6.31	0.03
	γ	64.19	24.24	2.92	3.12	6.43	0.69

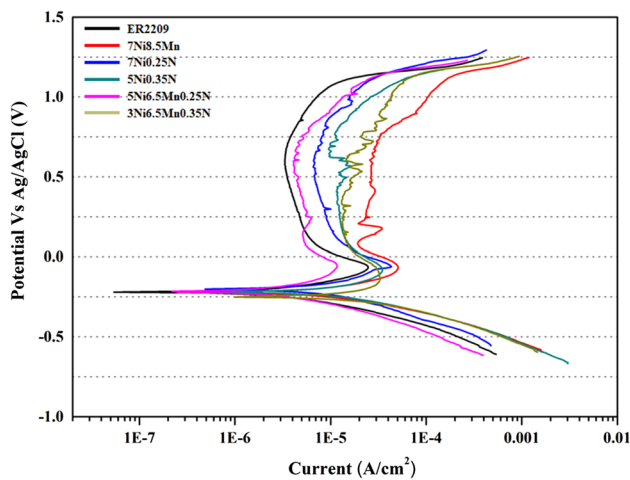


Fig. 5 Representative potentiodynamic polarization curves of weld metal measured in the 1.0M NaCl + 0.5M HCl solution

developed filler metals, the lower I_{pass} of 5Ni6.5Mn0.25N containing both Mn and N than 5Ni0.35N with the highest N indicates that there are factors affecting corrosion resistance other than PREN of the alloy. E_{trans} , which was a measure of the potential where the passive film broke down, showed similar values of approximately 1.1 V for all filler metals. However, for 7Ni8.5Mn and 3Ni6.5Mn0.35 N, the current slightly increased at 0.75 V and 0.6 V, respectively. Therefore, it can be said that these two filler metals have relatively low corrosion resistance compared to other filler metals. It is considered that the decrease in corrosion resistance is due to the difference in the PREN, and the PREN value of each phase was calculated using the austenite and ferrite chemical compositions measured by EPMA, as shown in Table 4. In duplex stainless steels, nitrogen was mostly distributed in austenite [32], so PREN values were higher in austenite than in ferrite. In other words, when the nitrogen content of filler metal was 0.15 wt%, the nitrogen content of austenite was 0.3 wt% higher than that of ferrite, the PREN value of austenite was higher than that of ferrite by about 4. And when the nitrogen content of filler metal was 0.35 wt%, the PREN value of austenite was higher by 10. 7Ni8.5Mn had the lowest PREN values of both austenite and ferrite owing to its high Mn content, and thus showed the lowest corrosion resistance. In the case of 5Ni0.35N and 3Ni6.5Mn0.35N, although the PREN of ferrite was similar to that of ER2209 and the PREN of austenite was higher than that of ER2209, the results of potentiodynamic polarization experiments

Table 3 Numerical results of the potentiodynamic polarization tests

	ER2209	7Ni8.5Mn	7Ni0.25 N	5Ni0.35 N	5Ni6.5Mn0.25 N	3Ni6.5Mn0.35 N
I_{pass} (A/cm ²)	5.05 E ⁻⁶	1.94 E ⁻⁵	9.54 E ⁻⁶	1.25 E ⁻⁵	5.73 E ⁻⁶	1.34 E ⁻⁵
E_{trans} (V)	1.135	1.152	1.124	1.122	1.155	1.144

Table 4 PREN values of the ferrite (δ) and austenite (γ) phases of the as-welded specimens (PREN = Cr + 3.3 Mo + 16N–Mn, wt%)

	Phase	PREN
ER2209	δ	31.48
	γ	35.19
7Ni8.5Mn	δ	24.81
	γ	28.71
7Ni0.25N	δ	31.65
	γ	38.68
5Ni0.35N	δ	31.67
	γ	41.27
5Ni6.5Mn0.25N	δ	27.55
	γ	33.63
3Ni6.5Mn0.35N	δ	28.08
	γ	38.51

showed that the corrosion resistance was lower than ER2209. Although the PREN of the weld metal and the PREN of the constituent phases were not lower (or rather higher) than ER2209, the corrosion resistance was low because the PREN difference between austenite and ferrite was large. Because the difference in PREN between austenite and ferrite, that is, the difference in corrosion resistance between austenite and ferrite, was large, it was concluded that the overall corrosion resistance decreased [8, 33]. Therefore, the excellent corrosion resistance of DSS appeared when the PREN was high and the corrosion resistance between austenite and ferrite was balanced.

Figure 6 shows the Vickers hardness values of the weld metals. The hardness of 7Ni8.5Mn was the highest and 7Ni0.25N was the lowest and the difference was about 6%. All filler metals had no microstructural differences and as shown in the XRD analysis results, there was no precipitation that could increase the hardness. Therefore, the difference of hardness was caused by the difference in chemical composition of filler metal. To maintain the phase fraction of weld metal, Ni in ER2209 was reduced by 2–6 wt%, and Mn and N were increased by 5–7 wt% and 0.1–0.2 wt%, respectively. 2 wt% or more of Mn was added to replace 1 wt% of Ni, indicating an increase in the substitutional alloying element of the filler metals. As the substitutional alloying elements increased, solid solution hardening occurred more and the hardness increased. There was almost no difference in hardness between ER2209 and 7Ni0.25N, indicating that 2 wt% of Ni and 0.1 wt% of N caused almost equal

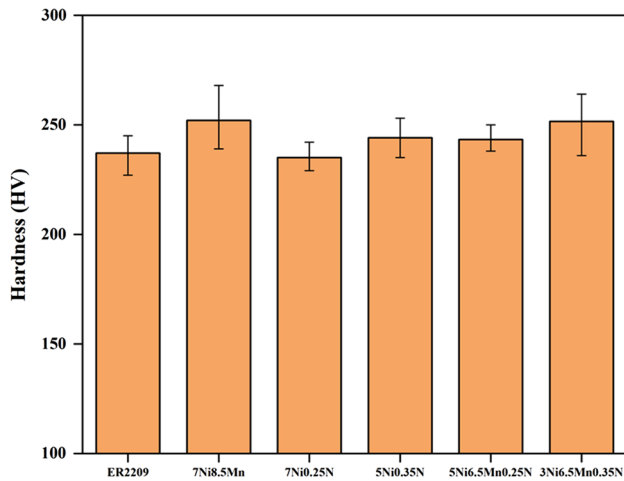


Fig. 6 Vickers hardness of as-welded filler metals

hardness increase. However, in 7Ni0.25N/5Ni0.35N and 5Ni6.5Mn0.25N/3Ni6.5Mn0.35N, the hardness increased even though Ni decreased by 2 wt% and N increased by 0.1 wt%. The solubility of N in most austenitic stainless steel is about 0.4 wt% [34]. As shown in Table 2, N in DSS was mostly distributed in austenite. So when the N content of the filler metals was 0.35 wt%, the N content of austenite was 0.7 wt%. In other words, N exceeding the solubility limit was supersaturated by the rapid cooling rate and the hardness increased. The hardness of 5Ni6.5Mn0.25N was rather decreased compared to 7Ni8.5Mn, because Mn increased the solubility of N and the Mn content decreased by 2 wt%. As a result, the hardness increased as Ni was replaced with Mn and also the hardness increased when N was added to exceed the solubility.

Figure 7 shows the results of the tensile tests of the weld metals. As described above, this is the tensile test results of all weld metals, excluding the effects of the base metal and HAZ. It indicated that the elongation of the filler metals was inversely proportional to the hardness. In addition, dynamic strain aging (DSA), which is uncommon at room temperature, was showed. It has been reported that DSA is a phenomenon caused by the interaction between diffusion solute atoms and mobile dislocations during plastic deformation, and DSA generally occurs at high temperature [35, 36]. At room temperature, DSA has been also reported to occur in austenitic stainless steel that exhibit deformation-induced martensitic transformation (DIMIT) [37, 38]. However, because the austenite of the filler metals used in this study is stable due to the high austenite stabilizer, the effect of DIMIT can be excluded. Kim et al. reported that the addition of N retards the DSA [38, 39]. However, DSA was observed in 7Ni0.25N and 5Ni0.35N whereas it was not observed in 5Ni6.5Mn0.25N and 3Ni6.5Mn0.35N, so it is difficult to explain only the effect of N content. Peng et al. reported that

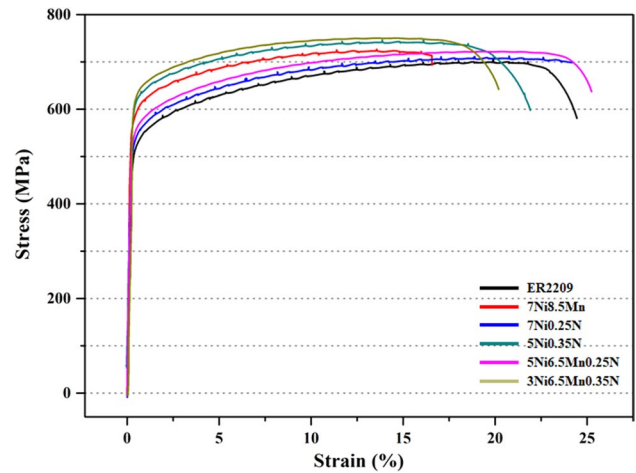


Fig. 7 Engineering stress–strain curves of filler metal with all-weld metal gauge length

Ni caused serrated flow at relatively low temperature [40]. Therefore, it was determined that DSA occurred due to the complex effect of N and Ni of filler metals. In addition, it is also necessary to investigate the influence of solute atoms such as Cr, Mn and the effect of slip band to understanding cause of DSA at room temperature. The tensile strength, yield strength, and elongation of the weld metals are summarized in Fig. 8 and Table 5. The developed filler metals showed higher tensile strengths than ER2209 because of the solid solution hardening effect due to the increase of substitutional and interstitial solute. The tensile strengths of filler metals ranged from 705 to 750 MPa, and there was a difference of about 6% between the minimum and maximum tensile strengths and this difference showed a similar tendency to hardness. In addition, the hardness and tensile strength showed the correlation suggested by Ashby and Jones [41]

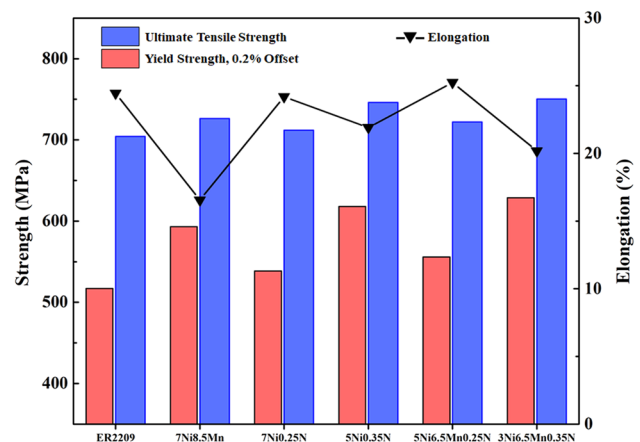


Fig. 8 Summary of tensile test for filler metals; tensile strength, yield strength, elongation

Table 5 Numerical results of the tensile tests for DSS filler metals

	Tensile strength (MPa)	Yield strength (MPa)	Elongation (%)
ER2209	704.2	517.2	24.5
7Ni8.5Mn	726.5	593.2	16.6
7Ni0.25N	711.9	538.6	24.2
5Ni0.35N	746.2	618.1	21.9
5Ni6.5Mn0.25N	722.0	555.8	25.2
3Ni6.5Mn0.35N	750.5	628.8	20.2

and Tabor [42]. However, the yield strengths showed a large difference depending on the chemical composition. The difference between the minimum and maximum yield strength was about 20%. From these results, it showed that the addition of Mn and N caused less work hardening. In particular, when 0.35 wt% of N was added, work hardening was significantly reduced.

Figure 9 shows the nanoindentation curves of ER2209 with the lowest yield and tensile strength and 3Ni6.5Mn0.35N with the highest yield and tensile strength. In ER2209, Fig. 9a, there was almost no difference in the nanoindentation curves between the as-welded ferrite and ferrite after the tensile test. However, the difference in the nanoindentation curves between the as-welded austenite and austenite after the tensile test was large. As shown in the nanoindentation curve in the as-welded condition of austenite, the displacement at the peak load was approximately 300 nm, and when the load was removed, the final displacement was approximately 275 nm. The results after

the tensile test showed that the displacement at the peak load was approximately 270 nm, and when the load was removed, the displacement was 240 nm, which was approximately 35 nm lower than that of the as-welded condition. This indicates that the hardness of austenite was higher after the tensile test than when it was as-welded, which was due to work hardening that occurred during the tensile test. In addition, because there was little difference between the nanoindentation curves of the as-welded condition and after the tensile test of ferrite, it indicates that work hardening hardly occurred in ferrite. This was caused by the difference in the work hardening capacity of austenite and ferrite. In general, it is well known that ferrite has a higher stacking fault energy (SFE) than austenite [42, 43]. As the SFE increases the work hardening capacity decreases, so the work hardening capacity of ferrite was lower than that of austenite [44, 45]. In addition, austenite and ferrite were already work hardened in the as welded state because thermal stress was applied to the weld metals by the welding process. Since the ferrite had a low work hardening capacity, it was sufficiently hardened in the as welded state. As a result, there was little increase in hardness even after tensile test. On the other hand, austenite remained the capacity to be work hardened even after hardening by thermal stress, so the hardness was increased by the tensile test. The nanoindentation curves of 3Ni6.5Mn0.35N, Fig. 9b, shows that curves of both austenite and ferrite overlapped under the as-welded condition and after the tensile test. The high content of solute atoms contained in 3Ni6.5Mn0.35N increased the dislocation density for a given deformation [46]. It caused an increase in the hardness of austenite in the as welded state, and less work hardening occurred during the tensile test.

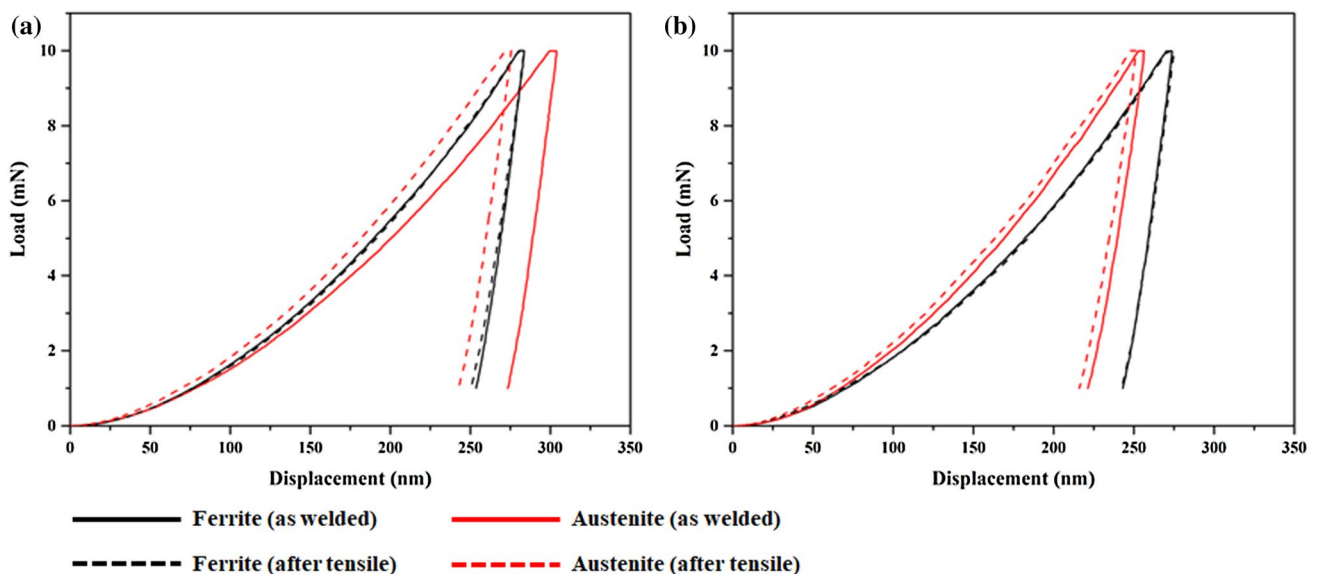
**Fig. 9** Representative P–h curves of ferrite and austenite; as welded (solid line) and after tensile test (dotted line) **a** ER2209, **b** 3Ni6.5Mn0.35N

Figure 10 shows the hardness of austenite and ferrite in the as-welded state and after the tensile test of all the filler metals obtained through nanoindentation experiments. In the case of ER2209, a commercial filler metal, the hardness of ferrite was higher than that of austenite in the as-welded state, and the hardness of austenite significantly increased by work hardening after the tensile test. In all filler metals, the hardness of ferrite in the as-welded state and after the tensile test was not large because strain hardening hardly occurred due to the low work hardening capacity in ferrite. In the developed filler metals, the hardness of austenite was higher than that of ferrite because of the solid-solution hardening effect of austenite stabilizers Mn and N in the as-welded state. Among them, 7Ni8.5Mn and 5Ni0.35N and 3Ni6.5Mn0.35N showed much higher hardness of austenite than ferrite in the as-welded state. In addition, the austenite of these filler metals did not significantly increase in hardness even after tensile test. That is, the austenite containing relatively high solute atoms was hardened by thermal stress caused by welding process in the as welded state, making it a harder phase than ferrite. As shown in Fig. 7 and Table 5, filler metals containing a large amount of Mn and N (7Ni8.5Mn, 5Ni0.35N, and 3Ni6.5Mn0.35N) had high yield strength. And these filler metals had similar tensile strength to that of filler metals with a low yield strength (ER2209, 7Ni0.25N and 5Ni6.5Mn0.25N). This was the result of less work hardening in austenite that was already hardened in the as welded state. In contrast, in the case of ER2209, 7Ni0.25N, and 5Ni6.5Mn0.25N, which had low austenite hardness in the as-welded state, the yield strength was low and the austenite hardness significantly increased after the tensile test, indicating that work hardening significantly occurred in the austenite.

Figure 11 shows the microstructure of the cross-section after the tensile test using SEM. In general, cracks in duplex stainless steel are known to occur at the austenite and ferrite phase boundaries [47, 48]. Whereas, in the case of filler metals in which austenite became a harder phase (7Ni8.5Mn, 5Ni0.35N, 3Ni6.5Mn0.35N), cracks or voids were generated inside the austenite. The reason for the high hardness of austenite in the as-welded state is considered that the high dislocation density of austenite containing large amount of alloying elements (Mn and N). During tensile test, stress was concentrated inside the austenite with high dislocation density and cracks occurred. Consequently, the yield strength and elongation of the duplex stainless steel weld metals in which Ni was replaced with Mn and N were determined by the intrinsic properties of austenite. The corrosion resistance did not significantly decrease when Ni was replaced with Mn or N. Therefore, it was shown that if the properties of austenite are controlled in the duplex stainless steel weld metal, Ni can be sufficiently replaced by Mn and N without significant deterioration of the overall filler metal properties.

4 Conclusions

In this study, Ni was replaced with Mn and N, and the effect of the changes in the intrinsic properties of austenite and ferrite in the duplex stainless steel weldment where the phase fraction was maintained at 50:50 was studied, including the mechanical properties and corrosion resistance of the entire weldment. As a result, the possibility of replacing Ni with Mn and N was suggested, and the detailed results are as follows:

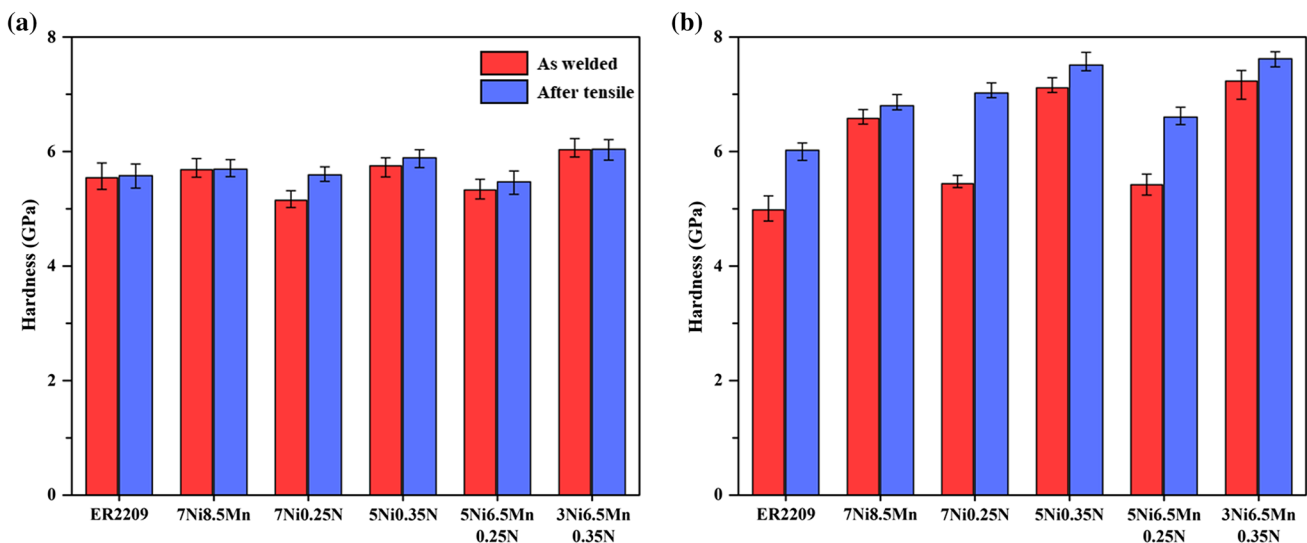


Fig. 10 Hardness of each phase obtained by the nanoindentation test; **a** ferrite, **b** austenite

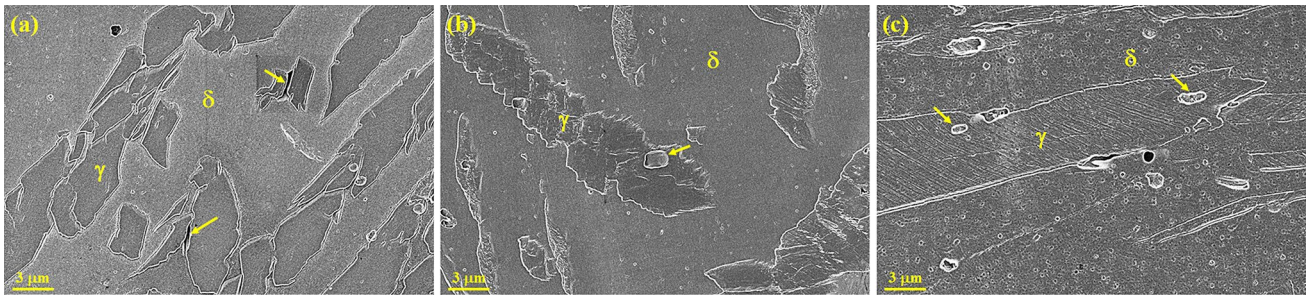


Fig. 11 Micrographs of the cross-section area for the tensile tested specimens of **a** 7Ni8.5Mn, **b** 5Ni0.35N, and **c** 3Ni6.5Mn0.35N

1. The five alloys in which Ni was replaced by Mn, N, and Mn + N were designed using the Delong diagram, which is a classical method for predicting the phase fraction of the weld and Thermo-Calc calculation. In the Delong diagram, 2 wt% Mn per 1 wt% Ni was sufficient. However, in order to maintain the phase fraction of the weldments at 50:50, it was necessary to add more than 2 wt% Mn per 1 wt% Ni. As a result of microstructure observation, GBA, WA, and IGA, which are generally found in duplex stainless steel weldments, were present in the ferrite matrix, and no precipitation or secondary phase was degrading the properties.
2. The passive region of all alloys was 0.1–1.15 V and the tendency to form a passive film was similar, so it is presumed that the decrease in corrosion resistance was not significant. However, 7Ni8.5Mn and 3Ni6.5Mn0.35N had a section in which the current value slightly increased before reaching 1.15 V, which can be said to have relatively low corrosion resistance compared to other alloys. In the case of 7Ni8.5Mn, this is due to the low PREN and the high Mn content, and in the case of 3Ni6.5Mn0.35N, the difference in corrosion resistance between austenite and ferrite was too large.
3. The tensile test results showed that the yield strength, tensile strength and elongation of the duplex stainless steel weldment were related to changes in the intrinsic properties of austenite. The hardness of the as-welded ferrite measured through nanoindentation did not significantly vary depending on the alloying element, but the hardness of austenite differed according to the alloying element. In the case of the filler metal containing a large amount of Mn and N, the hardness of austenite was high in the as-welded state, and thus the yield strength was also high. In addition, as a result of observing the cross-section after the tensile test, the filler metals with high yield strength had a fracture initiation inside the austenite, which resulted in low elongation. It is judged that additional research is needed on the change in the hardness of austenite according to the chemical composition and different deformation behavior of austenite

and ferrite during the tensile test. In summary, when Ni was replaced with Mn or N excessively, the hardness of austenite increased and elongation of weld metals decreased. Therefore, it is necessary to replace Ni with Mn + N to retain its mechanical properties and corrosion resistance.

Acknowledgements This study was supported financially by the Ministry of Trade, Industry & Energy (MI, Republic of Korea) under Strategic Core Materials Technology Development Program (No. 10067375).

Author Contributions All authors contributed to the study conception and design. Material preparation was performed by JM and T-HL. Data collection and analysis were performed by YL, JHL and CL. The first draft of the manuscript was written by YL and all authors commented on previous versions of the manuscript. All authors read and approved the final manuscript.

Funding This work was supported by Ministry of Trade, Industry & Energy (MI, Republic of Korea) under Strategic Core Materials Technology Development Program (No. 10067375).

Availability of Data and Material The datasets obtained from this study and the analyzed results during current research work are available from the corresponding author upon reasonable request.

Declarations

Conflict of interest The authors declare that they have no known competing financial interests or personal relationships that could have appeared to influence the work reported in this paper.

References

1. D. Escriba, E. Materna-Morris, R. Plaut, A. Padilha, *Mater. Charact.* **60**, 1214 (2009)
2. C. Rubio-González, C. Felix-Martinez, G. Gomez-Rosas, J. Ocaña, M. Morales, J. Porro, *Mater. Sci. Eng. A* **528**, 914 (2011)
3. J. Verma, R.V. Taiwade, *J. Manuf. Process.* **25**, 134 (2017)
4. W. Luu, P. Liu, J. Wu, *Corros. Sci.* **44**, 1783 (2002)
5. V. Moura, L. Lima, J. Pardal, A. Kina, R. Corte, S. Tavares, *Mater. Charact.* **59**, 1127 (2008)
6. C. Herrera, D. Ponge, D. Raabe, *Acta Mater.* **59**, 4653 (2011)

7. H. Luo, X. Li, C. Dong, K. Xiao, Arab. J. Chem. **10**, S90 (2017)
8. S.-T. Kim, S.-H. Jang, I.-S. Lee, Y.-S. Park, Corros. Sci. **53**, 1939 (2011)
9. D. Kang, H. Lee, Corros. Sci. **74**, 396 (2013)
10. G. Chail, P. Kangas, Proc. Struct. Integ. **2**, 1755 (2016)
11. M. Sadeghian, M. Shamanian, A. Shafyei, Mater. Design **60**, 678 (2014)
12. Technical Marketing Resources, Inc., *Practical Guidelines for the Fabrication of Duplex Stainless Steels*, 1st edn. (London, IMO: International Molybdenum Association 1999)
13. A. Kellai, A. Lounis, S. Kahla, B. Idir, Int. J. Adv. Manuf. Technol. **95**, 3215 (2018)
14. V. Muthupandi, P.B. Srinivasan, S. Seshadri, S. Sundaresan, Mater. Sci. Eng. A **358**, 9 (2003)
15. S. Geng, J. Sun, L. Guo, H. Wang, J. Manuf. Process. **19**, 32 (2015)
16. Z. Zhang, H. Jing, L. Xu, Y. Han, G. Li, L. Zhao, J. Mater. Eng. Perform. **26**, 134 (2017)
17. A. Ramirez, J. Lippold, S. Brandi, Metall. Mater. Trans. A **34**, 1575 (2003)
18. L. Karlsson, Weld. World **56**, 65 (2012)
19. W. Liu, Y. Zheng, C. Liu, Z. Yao, W. Ke, Wear **254**, 713 (2003)
20. H.-Y. Ha, T.-H. Lee, C.-S. Oh, S.-J. Kim, Scripta Mater. **61**, 121 (2009)
21. M. Pozuelo, J. Wittig, J.A. Jiménez, G. Frommeyer, Metall. Mater. Trans. A **40**, 1826 (2009)
22. H.-Y. Ha, M.-H. Jang, T.-H. Lee, Electrochim. Acta **191**, 864 (2016)
23. J. Yoo, K. Han, Y. Park, J. Choi, C. Lee, Sci. Technol. Weld. Joi. **19**, 514 (2014)
24. J.W. Simmons, B.S. Covino Jr., J.A. Hawk, J.S. Dunning, ISIJ Int. **36**, 846 (1996)
25. J. Li, Y. Xu, X. Xiao, J. Zhao, L. Jiang, J. Hu, Mater. Sci. Eng. A **527**, 245 (2009)
26. V. Muthupandi, P.B. Srinivasan, S. Seshadri, S. Sundaresan, Corrosion Eng. Sci. Technol. **38**, 303 (2003)
27. K. Migiakis, G. Papadimitriou, J. Mater. Sci. **44**, 6372 (2009)
28. R.-I. Hsieh, H.-Y. Liou, Y.-T. Pan, J. Mater. Eng. Perform. **10**, 526 (2001)
29. J. Potgieter, P. Olubambi, L. Cornish, C. Machio, E.-S.M. Sherif, Corros. Sci. **50**, 2572 (2008)
30. H.-Y. Ha, M.-H. Jang, T.-H. Lee, J. Moon, Corros. Sci. **89**, 154 (2014)
31. N. Suutala, Metall. Trans. A **13**, 2121 (1982)
32. M.-H. Jang, J. Moon, T.-H. Lee, S.-J. Park, H.N. Han, Metall. Mater. Trans. A **45**, 1653 (2014)
33. H. Park, J. Corrosion Sci. Soc. Korea **28**, 78 (1999)
34. J. Simmons, Mater. Sci. Eng. A **207**, 159 (1996)
35. S.-G. Hong, S.-B. Lee, J. Nucl. Mater. **328**, 232 (2004)
36. J.-H. Shin, G.-Y. Rim, S.-D. Kim, J.H. Jang, S.-J. Park, J. Lee, Mater. Charact. **164**, 110316 (2020)
37. M. Wendler, M. Hauser, O. Fabrichnaya, L. Krüger, A. Weiß, J. Mola, Mater. Sci. Eng. A **645**, 28 (2015)
38. J. Mola, G. Luan, Q. Huang, C. Ullrich, O. Volkova, Y. Estrin, Acta Mater. **212**, 116888 (2021)
39. D.W. Kim, W.G. Kim, W.-S. Ryu, Int. J. Fatigue **25**, 1203 (2003)
40. K. Peng, K. Qian, W. Chen, Mater. Sci. Eng. A **379**, 372 (2004)
41. M.F. Ashby, D.R. Jones, *Engineering Materials 1: An Introduction to Properties, Applications and Design* (Elsevier, Amsterdam, 2012)
42. D. Tabor, *The Hardness of Metals* (Oxford University Press, Oxford, 2000)
43. S. Pramanik, S. Bera, S.K. Ghosh, Steel Res. Int. **85**, 776 (2014)
44. W. Reick, M. Pohl, A.F. Padilha, Steel Res. **67**, 253 (1996)
45. R. Xiong, H. Peng, S. Wang, H. Si, Y. Wen, Mater. Design **85**, 707 (2015)
46. B. Verlinden, J. Driver, I. Samajdar, R.D. Doherty, *Thermo-Mechanical Processing of Metallic Materials* (Elsevier, Amsterdam, 2007), pp.57-69
47. I. Alvarez-Armas, M. Marinelli, J. Malarrí, S. Degallaix, A. Armas, Int. J. Fatigue **29**, 758 (2007)
48. E.-Y. Guo, M.-Y. Wang, T. Jing, N. Chawla, Mater. Sci. Eng. A **580**, 159 (2013)

Publisher's Note Springer Nature remains neutral with regard to jurisdictional claims in published maps and institutional affiliations.